ACS OMEGA

Open Access

http://pubs.acs.org/journal/acsodf

Article

X-ray Attenuating Vesicles with Neutrophil Extracellular Trap (NET) Specificity: Synthesis and Testing in a Model System

Mark Epshtein, Matthew J. Gounis, and Alexei A. Bogdanov, Jr.*

Cite This: *ACS Omega* 2024, 9, 29391−29400

Read Online

ACCESS | Metrics & More | Article Recommendations | Supporting Information

ABSTRACT: X-ray attenuating contrast agents for imaging thrombi directly during endovascular thrombectomy (EVT) are urgently needed for shortening the wait time for treatment and for reducing the chances of blood clot fragmentation. Neutrophil extracellular traps (NETs) are a product of an innate immune system response by which neutrophils release decondensed chromatin strands decorated with granule and cytosolic proteins, including neutrophil elastase and citrullinated histone H3 (CitH3). NETs are frequently found within fibrous thrombi in pathology and represent a promising target for thrombi-specific imaging agents due to their common occurrence in human cerebrovascular thrombi. We designed and tested 200 nm lipid vesicles (LV) formulated in the presence of a combination of hydrophilic and hydrophobic computed tomography (CT) contrast agents with resultant efficacy of X-ray attenuation corresponding to 312 ± 54 mg/mL iodine. The LV incorporated *trans*-cyclooctene-terminated pegylated distearoylphosphatidylethanolamine (TCO-PEG-DSPE) for rapid conjugation of methyltetrazine(mTz)-modified monoclonal immunoglobulin G (IgG) with anti-citH3 binding specificity. By using differential fluorescent labeling of the antibody and lipid components, we determined that 80 ± 3% of mTz-linked IgG coprecipitated with the LV after conjugation in contrast to 0.1−0.2% of control IgG. The engineered NET-specific LV were tested in vitro using differentiated human HL60 promyeloblasts (dHL60) as a standard model of NETing neutrophils. Using fibrin meshwork-incorporated dHL60 as well as monolayer cell cultures, we determined that anti-citH3 LV showed specific and high-affinity binding to dHL60 cells, which were stimulated to undergo NETosis. This work suggests the high promise of NET-specific agents in providing thrombus-specific imaging contrast during EVT.

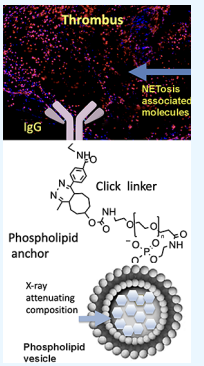

1. INTRODUCTION

Mechanical endovascular thrombectomy (EVT)- and tPA (tissue plasminogen activator)-mediated thrombolysis are two currently available state-of-the-art treatments for ischemic stroke. The EVT procedure has a very high success rate but relies on the knowledge of the thrombus location. The latter is determined by using digital subtraction angiography and requires the administration of an X-ray attenuating contrast agent. However, neither the length of the clot, i.e., the extension of the thrombus through the vessel, nor the formation of debris or clot location changes can be imaged directly[1] because blood clots do not attenuate X-rays. Meanwhile getting complete reperfusion on the first EVT attempt is known to improve outcomes[2] but remains a challenge. Thus, the ability to visualize and track blood clots in real-time during the procedure would be a major improvement, reducing the number of passes and shortening the wait time for treatment.

Fibrin- and GPIIb/IIIa (fibrinogen and Von Willebrand factor (VWF) specific platelet receptor) were, so far, commonly chosen as targets of imaging agents. These targets were favored during the development of imaging agents for positron emission tomography (PET), computed tomography (CT), and magnetic resonance imaging.[3] In particular, fibrin-binding polypeptides derived from phage or ribosome-display libraries have been studied as potential high-affinity thrombus-specific ligands.[4] However, most lysis-resistant clots requiring EVT have more platelet-rich areas with dense fibrin structures,[5] which are surrounded by neutrophil extracellular traps (NETs),[5−7] i.e., the obstacles for fibrin-specific agents. NETs are produced mainly due to peptidyl arginine deiminase 4 (PAD4)-mediated citrullination of H3 histones, which remain incorporated into the chromatin while externalized together with myeloperoxidase, elastase, and other granular and cytoplasmic proteins.[6,8] NETs are numerous in thrombi and are potentially accessible. Moreover, citrullinated H3-containing NETs may occupy up to 14% of the total thrombus volume.[9] The current availability of high-affinity antibodies to NET molecules and the feasibility of engineering suitable molecular mimics underscore the feasibility of NET-targeting for imaging thrombi.

Liposomes (lipid vesicles, LV) represent a well-established class of nanosized drug carrier vehicles capable of carrying high numbers of X-ray attenuating molecules within both the

Received: February 16, 2024
Revised: May 30, 2024
Accepted: June 10, 2024
Published: June 24, 2024

https://doi.org/10.1021/acsomega.4c01525
ACS Omega 2024, 9, 29391−29400

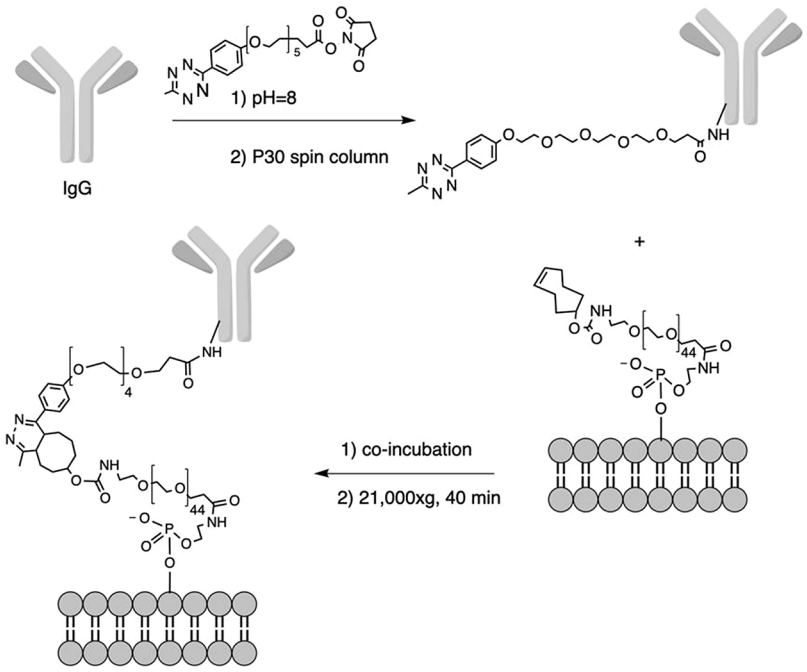

Figure 1. Schematic drawing showing covalent modification of IgG with methyltetrazine (mTz) residues with subsequent conjugation to TCO-PEG-DSPE -containing LV.

aqueous phase and in the lipid bilayer.[10] Furthermore, submicron-sized particles permeate the matrix and get retained within the clots.[11] The application of injection force mostly dislodges thrombus-associated inert particles[11] but receptor-bound particles such as platelets would remain bound.[12]

Since NETs are abundant in thrombi, we explored the covalent conjugation of NET-seeking antibodies to the surface of LV loaded with dual water-soluble as well as hydrophobic X-ray attenuating agents. These LV were studied as a prototype of a thrombus-specific contrast agent developed for the needs of EVT imaging. We also tested the specificity of binding to the NET components in a realistic model clot system.

2. MATERIALS AND METHODS

2.1. Synthesis of Lipids with Modified Headgroups. Synthesis of DSPE-Cy3 was performed by adding 1.5-fold molar excess of Cy3-NHS (10 μmol, Cyanine3 NHS ester, Lumiprobe) dissolved in 50 μL of DMSO to 1 mL of DSPE solution (5 mg/mL $CHCl_3$, 6.6 μmol) in the presence of 15 μL of *N*,*N*-diisopropylethylamine (DIPEA). The reaction mixture was stirred under argon for 2 h and subjected to flash column chromatography on Silicagel60 (5 g, Millipore-Sigma). The product was eluted using 20−25% methanol in $CHCl_3$. For the synthesis of TCO-PEG-DSPE (Figure S1), 25 μmol of TCO-PEG4-NHS (Click Chemistry Tools, Inc., Scottsdale AZ) in ethanol was added to a solution of 10 μmol DSPE-PEG(2000)Amine (Avanti Polar Lipids, Inc.) in 3 mL of $CHCl_3$ containing 50 μL of DIPEA. The completeness of amino group acylation was checked by using staining TLC plates (eluted with chloroform:methanol:ammonia, 65:25:4, see Supporting Information, Figure S2). The reaction mixture was dialyzed against 0.1 M NaCl overnight (MWCO 3000), lyophilized, and subjected to flash column chromatography on a 10 g Silicagel60 column equilibrated and flushed with ethyl acetate with subsequent elution of the product with 15% methanol in $CHCl_3$. The purity of the products was routinely checked by using TLC as described above and characterized using 500 MHz ^{1}H NMR (see Supporting Information, Figure S3).

2.2. Liposome Formulation. LV were formulated by dissolving a mixture of 82.5 μmol (65 mg/mL) of DSPC, 60 μmol (23 mg/mL) of cholesterol, 7.5 μmol (21 mg/mL) of DSPE-PEG2000, 1.9 μmol (6 mg/mL) of TCO-PEG-DSPE, and 4 μmol of DSPE-Cy3 in 5 mL of $CHCl_3$ and removing the solvent in vacuum. Control lipid films for LV were prepared by omitting TCO-PEG-DSPE and DSPE-PEG2000. For preparing LV containing dual contrast agents, an additional 126 μL ethiodized oil (480 mg/mL iodine, Lipiodol, Guerbet) was added to the lipid solution. The obtained lipid films were dissolved in 4 mL of *t*-butanol, snap-frozen, and lyophilized. The obtained powders were hydrated using 1 mL of concentrated clinical grade Iohexol solution (755 mg/mL iohexol, 350 mg/mL iodine, sterile filtered through a 0.2 μm PVDF membrane) at 65 °C for 30 min. The suspension was subjected to ultrasound homogenization in a thermostatic bath-type sonicator (Branson) at 60 °C for 30 min at the highest energy setting. The LV was passed through a series of Nuclepore membranes (1, 0.2, and 0.1 μm, Whatman) using a small-scale manual extrusion unit (LiposoFast, Sigma) at 60 °C. LV samples were analyzed by using dynamic light scattering (Zetasizer Nano ZS, Malvern) after diluting in an isosmotic solution of 0.5 M sucrose in DPBS (1:500 dilution). Sample particle morphology was analyzed by using cryoTEM (FEI Tecnai Spirit 12).

2.3. Protein Modification and Conjugation to LV. A schematic representation of protein modification with methyltetrazine (mTz) residues and their conjugation to LV is shown in Figure 1.

BSA-free Rabbit IgG Isotype Control (Invitrogen) was treated with a 3× molar excess of Alexa Fluor 647 NHS Ester (ThermoFisher) in 20 mM Hepes, 0.15 M NaCl, pH 7.5 (HBS) for 1 h followed by purification on Bio-Spin P30 mini-columns (Bio-Rad) equilibrated with HBS. Modification of

https://doi.org/10.1021/acsomega.4c01525
ACS Omega 2024, 9, 29391−29400

protein A/G (ThermoFisher) was performed using the same conditions. Methyltetrazine-PEG4-NHS Ester (mTz-PEG4-NHS) was added at a 10× molar excess from a solution in DMSO to AF647 modified proteins (IgG or protein A/G). After reacting for 30 min, AF647 and mTz-modified proteins were purified on Bio-Spin P30 mini-columns.

2.4. Conjugation to TCO-PEG-DSPE and LV. Ten μM solution of mTz-modified IgG-AF647 in HBS was mixed with 2 μM solution of TCO-PEG-DSPE in water at various molar ratios (1:1, 1:5, 1:10, IgG/lipid by moles). After 2 h incubation at RT, the solutions were diluted with 5% acetonitrile in 20 mM triethylammonium acetate (TEAA), pH 7 to 1 mL, and loaded on 0.2 mL microspin columns filled with C8-SepPak silica (Waters) equilibrated with 20 mM TEAA, 5%acetonitrile. Flow through was collected after 5 min centrifugation at 600 × *g*, followed by elution of C8-silica bound fraction with 60% acetonitrile, 0.1%SDS in 20 mM TEAA. Fractions were collected and concentrated on YM50 Amicon Ultra-4 centrifugal filter units (Millipore-Sigma), and the fluorescence of concentrated fractions was measured by using a Cary Eclipse spectrofluorometer (Agilent) at l_{ex} 650/l_{em} 700 nm and analyzed on 4−15% SDS-PAGE.

Conjugation to TCO-PEG-DSPE -containing LV was achieved by combining 0.2 mL of LV containing 0.85 μmol TCO-PEG-DSPE in 755 mg/mL iohexol with 30 μL (300 pmol) of mTz-IgG-AF647 or mTz-protein A/G-AF647. Alternatively, hydrophobized DSPE-conjugated IgG-AF647 was mixed with control liposomes that did not contain TCO-PEG-DSPE at the same molar ratio as described above. Reaction mixtures were incubated at room temperature for 24 h. Reaction mixtures were diluted 10× using HBS and centrifuged at 21,000 × *g* for 40 min. The precipitate contained IgG-conjugated LV. Aliquots of supernatants and precipitates were diluted at 1:100 with 1% Triton X-100, 0.1% SDS, and 50% methanol in DPBS, and fluorescence of Cy3 (lipid marker) was measured in the supernatant and the precipitate at l_{ex} 550/l_{em} 570 nm; fluorescence of AF647 (protein label) was measured as described above. Samples of LV conjugated with AF647-labeled proteins (100 μL, 5 μmol lipid) were supplemented with SDS (0.5% final concentration), 150 μL of chloroform/methanol (2:1, vol) was added, and after 5 min of vortexing, the samples were centrifuged 21,000 × *g* for 10 min. The upper phase and the interface were collected, dried under argon, redissolved in 10 mM Tris, 0.1% SDS, pH 6.8, and analyzed by gradient SDS-PAGE.

2.5. Cell Culture and Clot Models. HL60 cells (CCl-240, ATCC) were cultured in 10% FBS in Iscove's Modified Dulbecco's Medium (IMDM, Gibco). To induce differentiation of HL60 cells, they were cultured in the presence of 1.5% DMSO in IMDM for 7−8 days in a 5%CO_2 incubator at 37 °C. Cell differentiation was estimated by the percentage of the multilobed nuclei on Wright-Giemsa-stained cytology slides. NETing of differentiated HL60 (dHL60) cells was activated prior to or during the incorporation into the model clots (thrombi model) using phorbol 12-myristate 13-acetate (PMA, Millipore-Sigma).[13] Washed dHL60 cells (5 × 10^5 cells/mL) were incubated for 1 h in IMDM (serum-free) and then stimulated using 50 nM PMA (final concentration) in OptiMEM (Gibco, Thermo-Fisher) for 4 h for incorporating into the model fibrin clots. Cells were incorporated at 200,000 cells/mL into the solution of human fibrinogen (Sigma, > 80% clottable) in OptiMEM (final concentration—14 mg/mL), following a procedure described by us before.[14] PMA was added to the dHL60 suspension in fibrinogen solution immediately before mixing with human thrombin (Sigma, 20 U/mL, final concentration) for rapid clotting and to prevent cell precipitation. Alternatively, cells were activated with 50 nM PMA in OptiMEM for 4 h after seeding at the density of 40,000 cells/well into the poly-D-lysine coated 96-well plates to obtain attached monolayers of activated cells. Control cells were seeded in the plates in the absence of PMA using poly-D-lysine coated wells of 96-well plates. The presence of the NETs in cell monolayers and the model thrombi after dHL60 stimulation was verified by immunofluorescence of thin frozen sections by using an anti-MPO, antielastase, or anticitrullinated-H3 (citH3) antibody (0.1 μg/mL) followed by mouse antirabbit-Cy5.5 or -AF647 conjugate with counter-staining with DAPI to visualize the nuclei and extranuclear chromatin.

2.6. LV Binding to Cells, Frozen Clot Thin Sections, and Quantitation. Phospholipid concentration in the LV was determined by using the ferrothiocyanate method.[15] HL60 (nondifferentiated) or dHL60 cells were either treated with PMA or left untreated in control wells for 4 h. The cells were fixed in the wells of 96-well plates using 4% formaldehyde (EM Sciences)/DPBS for 20 min, washed with DPBS and blocked by using a 0.2% Tropix I-block (Thermo-Fisher), 2% intralipid (phospholipid-stabilized soybean oil, Millipore Sigma) in TBS (TI-TBS) for 2 h. Frozen sections were incubated in the same blocking solution before adding the LV. Cy3-lipid labeled Iohexol-containing anti-citH3-conjugated LV, control rabbit IgG-conjugated LV, or nonconjugated LV were diluted to the same lipid concentration (0.75 mM total lipid), then serially diluted using the blocking solution described above and added to the wells with fixed cells. Incubation with frozen sections was performed at a 0.1 mM total lipid. After 1 h incubation with agitation, the sections were fixed with 4% formaldehyde in DPBS and mounted in the presence of DAPI for fluorescent microscopy.

For measurement of LV-conjugated IgG binding to the cells, HL60 or dHL60 cells were plated at 10^5 cells/well onto poly-D-lysine coated 96-well Stripwell-microplates (High binding capacity, opaque, Costar 3923) in OptiMEM (Gibco, Thermo-Fisher), incubated for 1h at 37 °C, and PMA was added to achieve final concentration of 50 ng/mL. Cells were incubated for 4h in a CO_2 incubator at 37 °C and fixed with 4% formaldehyde (EM Sciences)/DPBS for 20 min. Fixed cells were treated with 1% BSA in DPBS overnight and then permeabilized for 1 h by using 0.25% cetyltrimethylammonium bromide, 0.5% Triton X-100 in 0.1 M Tris, pH 7 followed by washing with 0.2% Tropix I-block, 0.05% Tween-20 in TBS 4 times. LV linked to either anticitrullinated-H3 (citH3) rabbit IgG or control rabbit IgG were added to the wells at various dilutions in TI-TBS and incubated for 2 h, washed with TI-TBS 4 times. Antirabbit-alkaline phosphatase (AP) conjugate (Sigma-Aldrich) was added to the wells at the dilution of 1:1000 in 0.2% Tropix I-block, 0.05% Tween-20 in TBS. In separate wells of the plate, the same dilution of antirabbit-AP conjugate was used for adding to serially diluted rabbit IgG preabsorbed on the surface of the 96-well plate to obtain a calibration of AP-generated chemiluminescence signal vs IgG amount. The plates were incubated for 1 h with agitation and washed 4× with 0.2% Tropix I-block and 0.05% Tween-20 in TBS and phosphatase activity was determined by using chemiluminescence measurements at 15 min after the addition of the CDP-Star substrate (Thermo-Fisher) diluted 1:1 with 2 mM $MgCl_2$/TBS, pH 9.5 (SpectraMax M5 plate reader,

https://doi.org/10.1021/acsomega.4c01525
ACS Omega 2024, 9, 29391−29400

Molecular Devices). Using AP signal calibration against adsorbed rabbit IgG, we converted chemiluminescent signals into IgG equivalents (ng IgG) and determined effective equilibrium dissociation constants by using specific binding-one site least squares fit of data (Prism 10, GraphPad Software LLC).

3. RESULTS AND DISCUSSION

3.1. Characterization of LV Containing X-ray Attenuating Contrast Agents. Initially, we performed encapsulation of two X-ray attenuating agents in LV. According to dynamic light scattering (DLS) results, highly concentrated (755 mg/mL) clinical iodinated contrast agent iohexol in the presence of phospholipid/cholesterol mixture (150 mM) gave a single Z_{av} ~140−154 nm LV peak after the treatment with ultrasound followed by the series of extrusions at elevated temperature. Hydrodynamic diameters of various extruded and nonconjugated LV were similar if LV were diluted in an isosmotic 0.5 M sucrose/DPBS solution, Table 1. If in addition to water-soluble X-ray attenuating contrast agent iohexol, an FDA-approved ethiodized oil (lipiodol) was added to the lipid phase. DLS measurements showed a number diameter of 107 ± 26 nm and intensity diameter of 80 ± 9 nm potentially due to the input of smaller liposome-incorporated light scattering oil droplets. The obtained PEGylated LV were electron dense on cryogenic transmission electron microscopy (cryo-TEM), indicating efficient encapsulation of iohexol (Figure 2A). X-ray imaging experiments suggested that 100 nm Nuclepore membrane-sized LV obtained in the presence of both concentrated iohexol (350 mg iodine/mL) and lipiodol (480 mg iodine/mL) attenuate X-rays very efficiently (Figure 2B, C, sample L1) with the attenuation efficacy corresponding to a solution containing 65 ± 13 mg/mL iodine while nonpurified LV attenuated X-rays with the efficacy of 312 ± 54 mg/mL iodine solution. In the absence of lipiodol, the attenuation of LV was approximately 1.5 times less strong (sample L2, Figure 2B). Based on these quantitative imaging data, we concluded that the LV had a high 21.2 ± 0.6% encapsulation efficacy of the total X-ray attenuating iodine in the initial iohexol/lipiodol mixture.

Table 1. DLS of LV Formulated in the Presence of Iohexol or Iohexol/Lipiodol

sample LV, 150 μM lipid, 0.5 M sucrose/DPBS	Z_{av}, nm (dispersity)	hydrodynamic diameter, intensity (nm), mean ± SD	hydrodynamic diameter, number (nm), mean ± SD
control LV	122.2 (0.145)	139 ± 43	90 ± 11
iohexol-LV	154.7 (0.076)	163 ± 41	125 ± 18
iohexol/lipiodol-LV[a]	140.0 (0.252)	80 ± 9	107 ± 26
anti-citH3-iohexol/lipiodol-LV	176.4 (0.156)	201 ± 71	141 ± 15

[a]Lipiodol was added at 0.126 g/mL of LV containing approximately 152 μmol lipid.

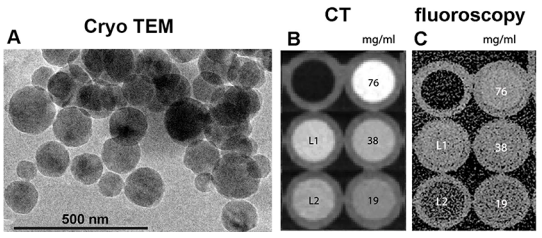

Figure 2. (A) CryoTEM image of LV obtained in the presence of 755 mg/mL iohexol. (B) CT image of LV samples in a 96-well plate and diluted iohexol standards (concentration is shown in mg iohexol/mL). L1−LV containing iohexol and lipoidol, L2−LV containing iohexol only. (C) Same set of samples as in (B) but imaged using standard fluoroscopy instrument. Bar = 500 nm.

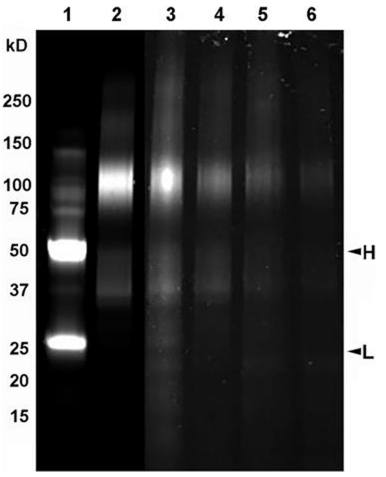

Figure 3. Gradient (4−15% acrylamide) SDS-PAGE analysis of DTT-reduced IgG-AF647 conjugated to TCO-PEG-DSPE. (1) non-conjugated mTz-IgG-AF647, (2) C8-silica flow-through fraction of PE-conjugated IgG-AF647 (molar ratio 1:1 IgG/PE); (3) C8-silica 60% acetonitrile/SDS eluted fraction (molar ratio 1:1 IgG/PE); (4) C8-silica flow-through fraction of PE-conjugated IgG-AF647 (molar ratio 1:5 IgG/PE); (5) C8-silica 60% acetonitrile/SDS eluted fraction (molar ratio 1:5 IgG/PE); (6) C8-silica 60% acetonitrile/SDS eluted fraction (molar ratio 1:10 IgG/PE). (H) Nonmodified heavy IgG chain; (L) nonmodified light IgG chain. MW markers are shown on the left.

3.2. Feasibility of Lipid Anchor Conjugation to AF647-Labeled and mTz-Modified Proteins. To achieve conjugation of antibodies or Fc-binding proteins with the LV we used highly efficient inverse electron-demand Diels−Alder (IEDDA) reaction known for rapid rate of selective reaction between *trans*-cyclooctene (TCO)- and tetrazines[16] resulting in high yields in various solvents, biological fluids and ultimately enabling in vivo applications.[17] The reaction rate and yield are important since ideally X-ray attenuating thrombus-specific agents should be assembled shortly before the interventional EVT procedure and used without purification. To test whether the interaction between (a) *trans*-cyclooctene-terminated (TCO) lipid incorporated into LV and mTz-modified model protein, or (b) lipid conjugated model protein and polyethylene glycol (PEG)-free LV would result in desired products, we performed several test experiments using distearoylphosphatidylethanolamine (DSPE)-PEG2000-amido-*trans*-cyclooctene (TCO-PEG-DSPE, see the Supporting Information, Figure S1) and mTz-modified model IgG (Figure 1) or recombinant protein AG.

To obtain the proof of conjugate formation between the lipid and protein components due to the IEDDA reaction we initially combined fluorescent-labeled mTz-modified rabbit IgG and purified DSPE-PEG2000-amido-*trans*-cyclooctene (TCO-PEG-DSPE) by coincubating of mTz-IgG-AF647 and TCO-PEG-DSPE micelles at various molar ratios (equimolar,

https://doi.org/10.1021/acsomega.4c01525
ACS Omega 2024, 9, 29391−29400

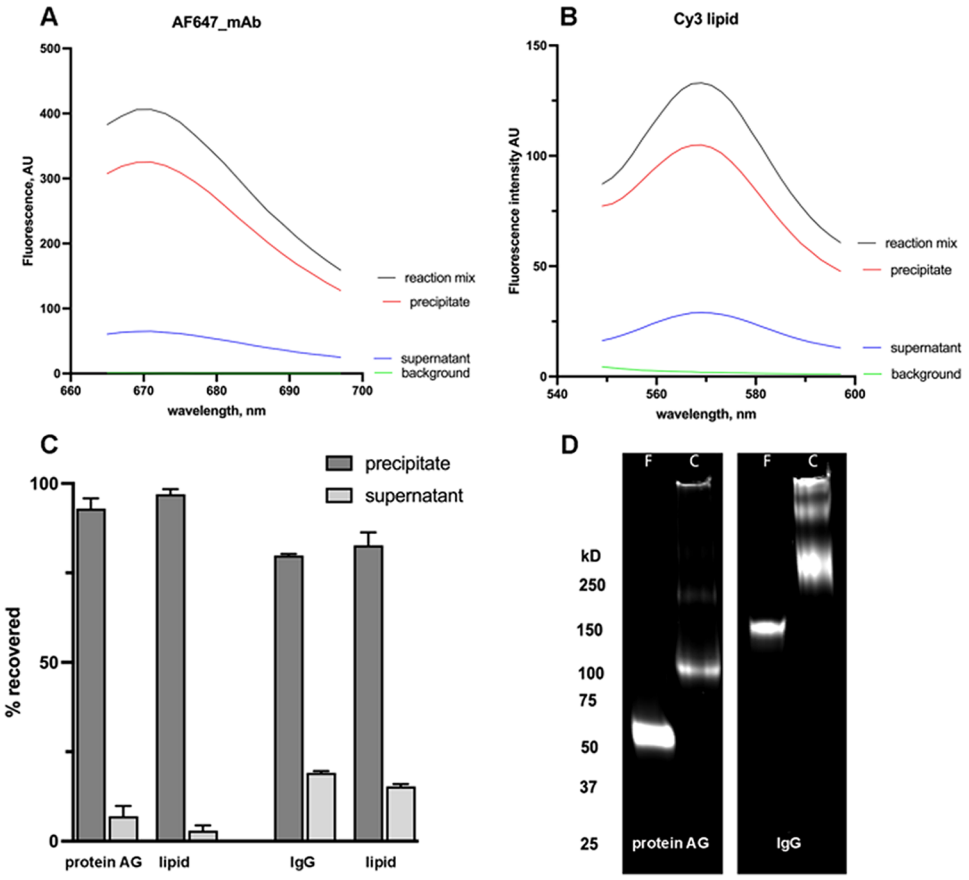

Figure 4. Conjugation of IgG and protein AG to TCO-PEG-DSPE containing LV. (A) Fluorescence spectra of reaction mixture as well as supernatant and precipitate fractions of LV-conjugated mTz-IgG-AF647; (B) fluorescence spectra of reaction mixture, supernatant, and precipitate fractions of Cy3-PE incorporated in to the LV lipid phase; (C) fractional content of IgG, protein AG and lipid in the precipitate (conjugated) and nonconjugated supernatant fraction, data shown as mean ± SD; (D) gradient SDS-PAGE, left panel—protein AG-AF647 as free control (F) and lipid-conjugated extracted from LV fraction (C), right panel—corresponding SDS-PAGE of IgG-AF647 (F—free, C—conjugated).

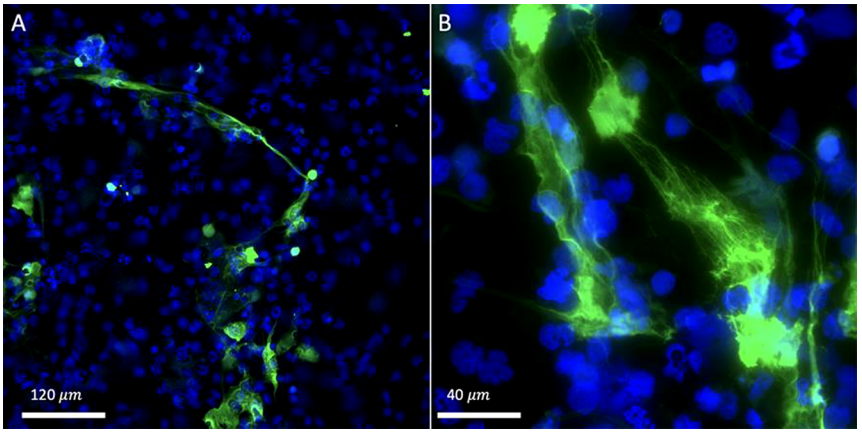

Figure 5. (A) Fluorescence microscopy of DMSO-differentiated HL60 cells (dHL60) stimulated by 50 nM phorbol 12-myristate 13-acetate (PMA) for 4 h. Substrate-attached cells were fixed and stained with the anti-citH3 antibody (green) and counterstained with DAPI (blue). (B) High-magnification image (right) shows extracellular DNA strands of NET-like structures partially decorated with citrullinated histone H3 (cyan color). Bar = 20 μm.

5- and 10- fold molar excess of TCO-PEG-DSPE over mTz-protein) at pH 7.5−8.[18] Conjugation reactions with either mTz-modified IgG, or protein AG, were set up immediately after the purification of mTz-modified proteins to minimize the effect of mTz hydrolysis. Spin-chromatography of lipid-modified IgG on 20 mM TEAA/5% acetonitrile-equilibrated C8-silicagel showed that 56−38% of the microcolumn-loaded fluorescent IgG was recovered in the flow-through fraction, while the rest of the IgG was recoverable with 60% acetonitrile and 0.1%SDS/20 mM TEAA in a denatured form. By using near-infrared (NIR) imaging of reducing SDS-PAGE of the flow-through as well as C8-column-retained fractions of lipid-conjugated IgG we determined that both heavy and light chains of IgG (H, L) were migrating slower than nonmodified

https://doi.org/10.1021/acsomega.4c01525
ACS Omega 2024, 9, 29391−29400

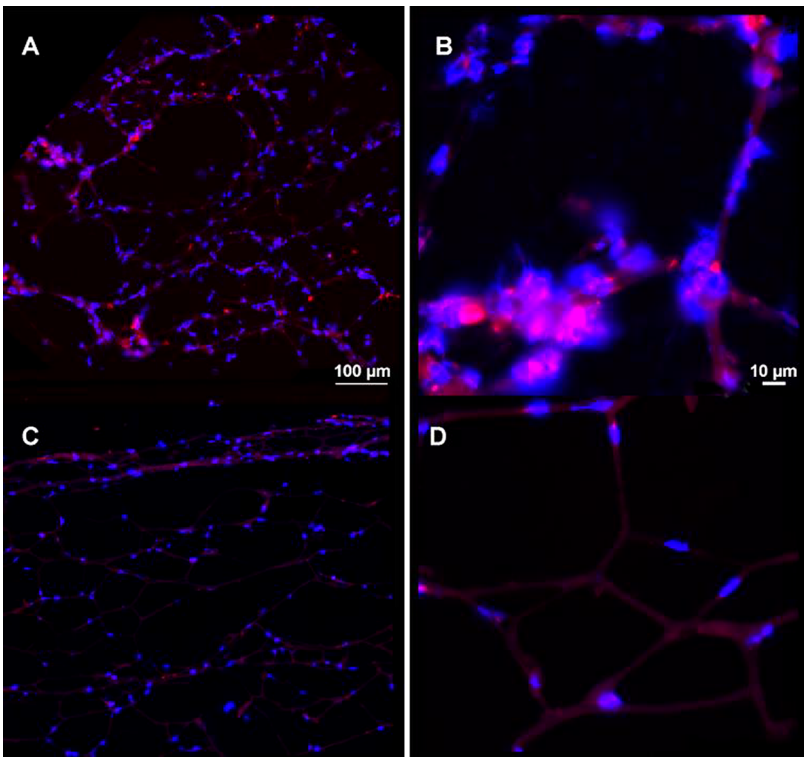

Figure 6. Immunofluorescent microscopy of thin frozen sections. Model fibrin clots contained dHL60 that were either stimulated with 50 nM PMA (A, B), or nonstimulated (C, D). Tiled 20× magnification images are shown in panels A and C, bar = 100 μm, high magnification (63×) representative images are shown in panels B (PMA stimulation) and D (control), bar = 10 μm. Pseudo colors: blue, nuclei stained with DAPI, red, anti-citH3 antibody (1:500 dilution) followed by goat-antirabbit-PE conjugate.

chains of DTT-reduced IgG (Figure 3) and that flow-through fraction of IgG modified with TCO-PEG-DSPE at the molar ratio of 1:1 contained no detectable nonmodified IgG chains (Figure 3, lane 1). Therefore, we obtained proof of conjugation of a TCO-terminated PEGylated lipid conjugation with mTz residues linked to the proteins.

Conjugation to X-ray attenuating LV was tested by coincubating mTz-IgG-AF647 with the iohexol/lipiodol-containing LV that had 3−4% of TCO-PEG-DSPE included in the lipid phase. The conjugation to these LV was complete at 2 h in the presence of a 10-fold molar excess of TCO-PEG-DSPE over mTz residues. We determined that the conjugation reaction resulted in high yields and did not require purification of LV from free iohexol as determined by diluting an aliquot of LV using isosmotic 0.5 M sucrose/DPBS buffer solution and precipitating the sample at 18,000 × *g*. Due to the high content of LV-trapped iohexol more than 85% of the lipid was sedimented after a 30 min centrifugation of LV diluted in an isosmotic buffer as shown by Cy3-conjugated lipid tracer fluorescence measurements (Figure 4A, B). According to the DLS data, the apparent hydrodynamic diameters of the obtained LV conjugate with monoclonal rabbit IgG increased by 30−40% with no aggregation (Table 1), which is consistent with the formation of protein-LV conjugates. As determined by fluorescence measurements which were performed separately for AF647 and Cy3 fluorophores, 80 ± 3% of AF647-tagged IgG coprecipitated with Cy3-labeled lipid (81 ± 2% Cy3-lipid tracer recovered in the LV precipitate), Figure 4B. Only 0.1−0.2% of control IgG-AF647 that was not modified with the mTz coprecipitated with the LV in a control experiment.

In experiments involving the mTz-modified protein AG-AF647, the conjugation to TCO-PEG-DSPE containing LV was even more efficient than IgG with 91 ± 2% of protein AG coprecipitating with the Cy3-lipid marker (Figure 4C). To confirm that the majority of IgG-AF647 and protein AG-AF647 were indeed conjugated to the lipids after their coprecipitation, we extracted precipitated LV with chloroform/methanol and analyzed separated water phase using SDS-gel electrophoresis (Figure 4D). In comparison to free nonconjugated fluorescent proteins, the LV-extracted hydrophobized proteins showed larger apparent masses and had slower electrophoretic migration, which is characteristic of the proteins with covalently linked lipids.[19]

The alternative to the covalent linking of proteins to LV is the spontaneous insertion of lipid-conjugated proteins (protein-lipopolymers) into the lipid phase of the LV.[20] For testing whether IgG-AF647 conjugated to TCO-PEG-DSPE would spontaneously incorporate into premade LV we performed coincubation of the flow-through fraction, which was obtained as the C8-silica flow-through fraction (Figure 3) with the control non-PEGylated LV. However, we found that a 24h 40 °C incubation did not result in an incorporation of IgG into the LV. While spontaneous insertion of hydrophobized proteins in the LV is an attractive alternative to conjugation to LV-incorporated reactive lipid headgroups,[20] the differences in properties of the proteins used in our study and previously studied much smaller protein/lipopolymer conjugates could be the reason for the lack of incorporation into the LV. Therefore, the IEDDA reaction between antibodies (or antibody-binding proteins) and TCO groups on the surface of premade LV appears to be an acceptable synthetic strategy leading to thrombus-targeted X-ray attenuating nanosized contrast agents.

https://doi.org/10.1021/acsomega.4c01525
ACS Omega 2024, 9, 29391−29400

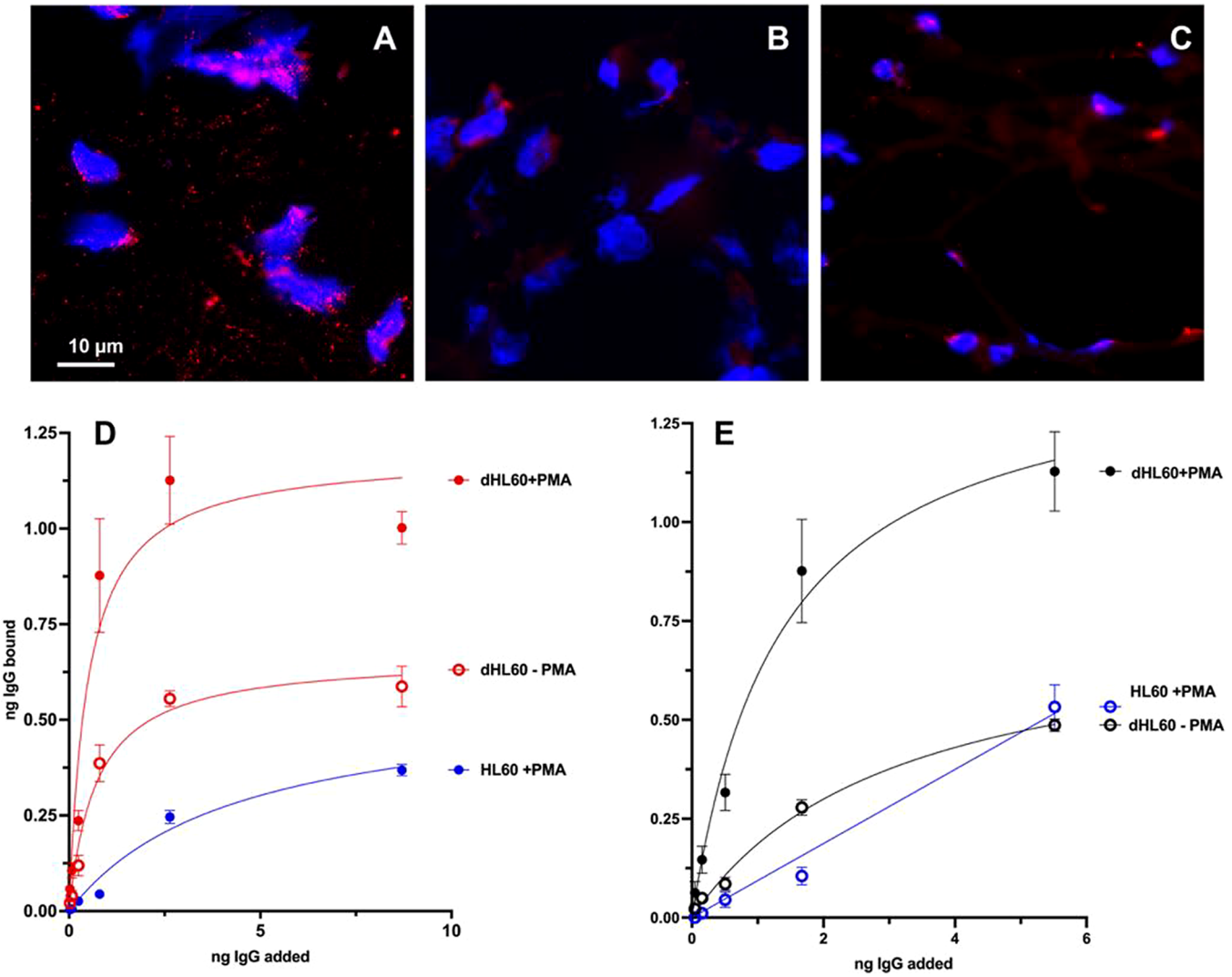

Figure 7. Binding of anti-citH3 IgG-conjugated LV to permeabilized dHL60 and HL60 cells in the presence or absence of PMA activation. Fluorescent microscopy of frozen sections of model fibrin clots incubated with anti-citH3 IgG-conjugated LV: (A) dHL60 cells activated with PMA (50 ng/mL) and incubated with anti-citH3 IgG-conjugated LV (0.1 mg lipid/mL); (B) nonactivated dHL60 cells and incubated with anti-citH3 IgG-conjugated LV; (C) control HL60 incubated with anti-citH3 IgG-conjugated LV, (red) Cy3-DSPE, (blue) DAPI, bar = 10 μm; (D) chemiluminescence-based quantitation of the binding of LV-conjugated anti-citH3 IgG to dHL60 or HL60 cells in the presence or the absence of PMA; (E) quantitation of the binding of LV-conjugated control rabbit IgG to dHL60 or HL60 cells in the presence or the absence of PMA.

3.3. Characterization of Model Systems Containing Incorporated dHL60 Cells. In further experiments differentiated human HL60 cells were used as a standard cell culture model of NETosis after phorbol 12-myristate 13-acetate (PMA) stimulation.[21] This model provides easy access to NET components that are present in human thrombi extracted by using the EVT procedure.[22] HL60 cells (dHL60) differentiated in suspension culture by using DMSO,[23] firmly attached to the cell culture plastic surfaces at 2−3 h after PMA addition. Control nonactivated dHL60 cells and HL60 cells grown in the absence of DMSO attached to the cell culture plastic after coating it with polylysine. The feasibility of detecting citrullinated (cit) proteins and simultaneous antibody testing in a model cell monolayer was demonstrated after a 4h PMA-induced NETosis of dHL60 cells. Approximately every 1 in 50 cells was stained positively anti-citH3 antibody (Figure 5A). In addition to the anti-citH3 antibody, binding extracellular structures formed by PMA-treated cells were positive for DAPI indicating classic extracellular chromatin trap formation (Figure 5B).[24] dHL60 were further incorporated in model fibrin clots either in the presence or the absence of PMA to provide a model of neutrophil infiltration and extracellular protein citrullination commonly occurring in human cerebrovascular thrombi.[25] Fluorescence microscopy of thin frozen sections identified cells attached to and incorporated into the fibrin meshwork with highly heterogeneous morphology of cell nuclei if the cells were stimulated with PMA before or during the model clot formation (Figure 6A, B) in comparison to control unstimulated dHL60 cells (Figure 6C, D). The presence of citrullinated proteins associated with the cells and around them was readily detectable on sections stained with anti-citH3 antibodies with the majority of antibodies reacting both with the components of fibrin bundles and with nuclei displaying dual fluorescence, suggesting citrullination of histones (Figure 6B).

3.4. Anti-citH3 LV Binding to Differentiated HL60 Cells. LV with conjugated anti-citH3 IgG (anti-citH3 LV) were tested in binding experiments involving thin frozen

https://doi.org/10.1021/acsomega.4c01525
ACS Omega 2024, 9, 29391−29400

sections of model fibrin clots with incorporated dHL60 cells pretreated with PMA to induce NETing (Figure 7A−C). Anti-citH3 LV containing lipid marker DSPE-Cy3 were incubated with the clot model sections in the presence of 1% BSA solution diluted with intralipid to minimize nonspecific binding of LV. Bright punctate red fluorescence was observed upon binding of fluorescent liposomes to the nuclei and around the periphery of dHL60 cells revealing potential externalized components of NETs (Figure 7A). In control binding experiments, we used clot-incorporated dHL60 cells (Figure 7B), which were not activated with PMA, or control nondifferentiated HL60 cells (Figure 7C). In both cases, only weak nonspecific fluorescence was detected.

The observed differences in fluorescence led us to quantify LV binding to dHL60 versus control HL60 cells in polylysine-coated 96 well plate surfaces. PMA activation of dHL60 cells resulted in NETing that was reflected in observed differences in the anti-citH3 IgG-mediated LV binding to fixed cell monolayers. To quantify the differences in binding of LVs to PMA-treated vs control cells we used alkaline-phosphatase (AP)-mediated chemiluminescence reflecting the binging of antirabbit IgG-AP conjugate at an optimized concentration to either anti-citH3 IgG, or nonspecific rabbit IgG-conjugated LV. Under the conditions of the assay, we measured the chemiluminescent signal proportional to the concentration of LV-conjugated IgGs which were associated with the cells (Figure 7D, E). The antirabbit IgG-AP conjugate alone had negligible levels of nonspecific binding to fixed HL60 cells. We showed that both LV types were associated with PMA-treated dHL60 cells if compared to nonactivated dHL60 controls, or alternatively, to nondifferentiated HL60 cells treated with PMA. However, anti-citH3 IgG-mediated LV binding showed at least 4 times higher apparent binding affinity than control IgG-linked LV with effective nonequilibrium dissociation constants (K_D^e) of 0.4 vs 1.6 nM, respectively. With no PMA treatment, the anti-citH3 IgG-conjugated LV have shown low levels of high-affinity binding (Figure 7D) possibly due to spontaneous NETing, while control rabbit IgG-linked LV showed nonspecific binding similar to PMA-treated non-differentiated HL60 cells (Figure 7E). It should be noted that observed rabbit IgG-linked LV binding to activated dHL60 cells could be caused by Fc receptor-mediated multipoint interaction with the LV due to the expression of a large number of Fc receptors (Fc gRIIA) by these cells.[26] In further experiments, the addition of an excess of nonspecific IgG-containing serum (which was omitted in our work) or enzymatic IgG fragmentation may be used for achieving higher specificity of interaction with NETing cells. Overall, our binding experiments showed that anti-citH3 IgG-conjugated LV exhibited higher affinity to NETs originating from activated dHL60 cells than control LV conjugated to nonspecific rabbit IgG.

4. CONCLUSIONS

In conclusion, we demonstrated that by loading both hydrophilic and lipophilic iodinated contrast agents into LV carrying reactive groups we obtained radiopaque and targetable NP. These LV had X-ray attenuating properties equivalent to 312 ± 54 mg/mL iodine solution; the use of high-yield and rapid metal-/azide-free click chemistry reaction between mTz-modified monoclonal anti-citH3 antibody and TCO-modified PEGylated lipid incorporated into the LV enabled efficient linking of IgGs recognizing externalized chromatin of NETing cells. We expect that due to the high yield of the conjugation reaction anti-citH3-LV may be used directly for specific imaging of the thrombi after local injection in situ due to the high-affinity binding of radiopaque LV to NETs.

■ ASSOCIATED CONTENT

Supporting Information

The Supporting Information is available free of charge at https://pubs.acs.org/doi/10.1021/acsomega.4c01525.

Additional figures; (1) representative structure of TCO-PEG2000-PE lipid anchor; (2) thin layer chromatography results; and (3) NMR spectrum of the lipid anchor (PDF)

■ AUTHOR INFORMATION

Corresponding Author

Alexei A. Bogdanov, Jr. − *Department of Radiology, New England Center for Stroke Research, and Cancer Center and Chemical Biology Interface Program, UMASS Chan Medical School, Worcester, Massachusetts 01655, United States;* orcid.org/0000-0003-4806-5869; Phone: (508)856-5571; Email: alexei.bogdanov@umassmed.edu

Authors

Mark Epshtein − *Department of Radiology and New England Center for Stroke Research, UMASS Chan Medical School, Worcester, Massachusetts 01655, United States*

Matthew J. Gounis − *Department of Radiology and New England Center for Stroke Research, UMASS Chan Medical School, Worcester, Massachusetts 01655, United States*

Complete contact information is available at: https://pubs.acs.org/10.1021/acsomega.4c01525

Notes

The authors declare no competing financial interest.

■ ACKNOWLEDGMENTS

We are grateful for the technical assistance with cell culture and microscopy provided by Ms. Anita Leporati. This work was funded in part by NIH grants 4RO1EB000851 (AAB) and 2R01NS105692 (MJG, consortium director; PI—Levitt). The project was supported also by the S10 OD025113 award to the UMass Electron Microscopy Core Facility (Research equipment grant).

■ ABBREVIATIONS

AF647, Alexa Fluor 647; CitH3, citrullinated histone H3; CT, computed tomography; Cryo TEM, cryogenic transmission electron microscopy; Cy3-NHS, cyanine 3 hydroxysuccinimide ester; dHL60, differentiated human promyelocytic leukemia HL60 cells; DSPC, distearoylphosphatidylcholine; DSPE, distearoylphosphatidylethanolamine; EVT, (mechanical) endovascular thrombectomy; IgG, immunoglobulin G; IEDDA, inverse electron-demand Diels−Alder; LV, lipid vesicle; mTz, methyltertrazine; NET, neutrophil extracellular trap; NHS, *N*-hydroxysuccinimide; NMR, nuclear magnetic resonance; PAD4, peptidyl arginine deiminase 4; PMA, phorbol 12-myristate 13-acetate; PET, positron emission tomography; TCO, *trans*-cyclooctene; TCO-PEG-DSPE, *trans*-cyclooctene-terminated pegylated distearoylphosphatidylethanolamine; tPA, tissue plasminogen activator; SDS-PAGE, sodium dodecyl

sulfate−polyacrylamide gel electrophoresis; vWF, von Willebrand factor.

REFERENCES

(1) Guo, S.; Guo, X.; Wang, X.; Zhou, D.; Du, X.; Han, M.; Zong, Y.; Wan, M. Reduced clot debris size in sonothrombolysis assisted with phase-change nanodroplets. *Ultrason Sonochem* **2019**, *54*, 183−191.

(2) Zaidat, O. O.; Castonguay, A. C.; Linfante, I.; Gupta, R.; Martin, C. O.; Holloway, W. E.; Mueller-Kronast, N.; English, J. D.; Dabus, G.; Malisch, T. W.; et al. First Pass Effect: A New Measure for Stroke Thrombectomy Devices. *Stroke* **2018**, *49* (3), 660−666.

(3) Botnar, R. M.; Perez, A. S.; Witte, S.; Wiethoff, A. J.; Laredo, J.; Hamilton, J.; Quist, W.; Parsons, E. C., Jr.; Vaidya, A.; Kolodziej, A.; et al. In vivo molecular imaging of acute and subacute thrombosis using a fibrin-binding magnetic resonance imaging contrast agent. *Circulation* **2004**, *109* (16), 2023−2029. Blasi, F.; Oliveira, B. L.; Rietz, T. A.; Rotile, N. J.; Day, H.; Looby, R. J.; Ay, I.; Caravan, P. Effect of Chelate Type and Radioisotope on the Imaging Efficacy of 4 Fibrin-Specific PET Probes. *J. Nucl. Med.* **2014**, *55* (7), 1157−1163. Von Zur Muhlen, C.; von Elverfeldt, D.; Moeller, J. A.; Choudhury, R. P.; Paul, D.; Hagemeyer, C. E.; Olschewski, M.; Becker, A.; Neudorfer, I.; Bassler, N.; et al. Magnetic resonance imaging contrast agent targeted toward activated platelets allows in vivo detection of thrombosis and monitoring of thrombolysis. *Circulation* **2008**, *118* (3), 258−267. Lohrke, J.; Siebeneicher, H.; Berger, M.; Reinhardt, M.; Berndt, M.; Mueller, A.; Zerna, M.; Koglin, N.; Oden, F.; Bauser, M.; et al. (18)F-GP1, a Novel PET Tracer Designed for High-Sensitivity, Low-Background Detection of Thrombi. *J. Nucl. Med.* **2017**, *58* (7), 1094−1099. Izquierdo-Garcia, D.; Desogere, P.; Philip, A. L.; Mekkaoui, C.; Weiner, R. B.; Catalano, O. A.; Iris Chen, Y. C.; DeFaria Yeh, D.; Mansour, M.; Catana, C.; et al. Detection and Characterization of Thrombosis in Humans Using Fibrin-Targeted Positron Emission Tomography and Magnetic Resonance. *JACC Cardiovasc Imaging* **2022**, *15* (3), 504−515.

(4) Oliveira, B. L.; Caravan, P. Peptide-based fibrin-targeting probes for thrombus imaging. *Dalton Trans* **2017**, *46* (42), 14488−14508. Petrokova, H.; Masek, J.; Kuchar, M.; Viteckova Wunschova, A.; Stikarova, J.; Bartheldyova, E.; Kulich, P.; Hubatka, F.; Kotoucek, J.; Knotigova, P. T. Targeting Human Thrombus by Liposomes Modified with Anti-Fibrin Protein Binders. *Pharmaceutics* **2019**, *11* (12), 642 DOI: 10.3390/pharmaceutics11120642.

(5) Staessens, S.; Denorme, F.; Francois, O.; Desender, L.; Dewaele, T.; Vanacker, P.; Deckmyn, H.; Vanhoorelbeke, K.; Andersson, T.; De Meyer, S. F. Structural analysis of ischemic stroke thrombi: histological indications for therapy resistance. *Haematologica* **2020**, *105* (2), 498−507.

(6) Varju, I.; Kolev, K. Networks that stop the flow: A fresh look at fibrin and neutrophil extracellular traps. *Thromb Res.* **2019**, *182*, 1−11.

(7) Novotny, J.; Oberdieck, P.; Titova, A.; Pelisek, J.; Chandraratne, S.; Nicol, P.; Hapfelmeier, A.; Joner, M.; Maegdefessel, L.; Poppert, H.; et al. Thrombus NET content is associated with clinical outcome in stroke and myocardial infarction. *Neurology* **2020**, *94* (22), e2346−e2360.

(8) Zuo, Y.; Zuo, M.; Yalavarthi, S.; Gockman, K.; Madison, J. A.; Shi, H.; Woodard, W.; Lezak, S. P.; Lugogo, N. L.; Knight, J. S.; et al. Neutrophil extracellular traps and thrombosis in COVID-19. *J. Thromb Thrombolysis* **2021**, *51* (2), 446−453.

(9) Laridan, E.; Denorme, F.; Desender, L.; Francois, O.; Andersson, T.; Deckmyn, H.; Vanhoorelbeke, K.; De Meyer, S. F. Neutrophil extracellular traps in ischemic stroke thrombi. *Ann. Neurol.* **2017**, *82* (2), 223−232.

(10) Kweon, S.; Lee, H. J.; Hyung, W. J.; Suh, J.; Lim, J. S.; Lim, S. J. Liposomes coloaded with iopamidol/lipiodol as a RES-targeted contrast agent for computed tomography imaging. *Pharm. Res.* **2010**, *27* (7), 1408−1415. Ghaghada, K. B.; Bhavane, R.; Badachhape, A.; Tanifum, E.; Annapragada, A. Nanoprobes for Computed Tomography and Magnetic Resonance Imaging in Atherosclerosis Research. *Methods Mol. Biol.* **2022**, *2419*, 809−823, DOI: 10.1007/978-1-0716-1924-7_49.

(11) Spero, R. C.; Sircar, R. K.; Schubert, R.; Taylor, R. M., 2nd; Wolberg, A. S.; Superfine, R. Nanoparticle diffusion measures bulk clot permeability. *Biophys. J.* **2011**, *101* (4), 943−950.

(12) Tandon, P.; Diamond, S. L. Hydrodynamic effects and receptor interactions of platelets and their aggregates in linear shear flow. *Biophys. J.* **1997**, *73* (5), 2819−2835.

(13) Guo, Y.; Gao, F.; Wang, Q.; Wang, K.; Pan, S.; Pan, Z.; Xu, S.; Li, L.; Zhao, D. Differentiation of HL-60 cells in serum-free hematopoietic cell media enhances the production of neutrophil extracellular traps. *Exp Ther Med.* **2021**, *21* (4), 353.

(14) Chueh, J. Y.; Wakhloo, A. K.; Gounis, M. J. Effectiveness of mechanical endovascular thrombectomy in a model system of cerebrovascular occlusion. *AJNR Am. J. Neuroradiol* **2012**, *33* (10), 1998−2003.

(15) Stewart, J. C. Colorimetric determination of phospholipids with ammonium ferrothiocyanate. *Anal. Biochem.* **1980**, *104* (1), 10−14.

(16) Blackman, M. L.; Royzen, M.; Fox, J. M. Tetrazine ligation: fast bioconjugation based on inverse-electron-demand Diels-Alder reactivity. *J. Am. Chem. Soc.* **2008**, *130* (41), 13518−13519.

(17) Zeglis, B. M.; Mohindra, P.; Weissmann, G. I.; Divilov, V.; Hilderbrand, S. A.; Weissleder, R.; Lewis, J. S. Modular strategy for the construction of radiometalated antibodies for positron emission tomography based on inverse electron demand Diels-Alder click chemistry. *Bioconjug Chem.* **2011**, *22* (10), 2048−2059.

(18) Bäuerle, T.; Gupta, S.; Zheng, S.; Seyler, L.; Leporati, A.; Marosfoi, M.; Maschauer, S.; Prante, O.; Caravan, P.; Bogdanov, A., Jr. Multimodal Bone Metastasis-associated Epidermal Growth Factor Receptor Imaging in an Orthotopic Rat Model. *Radiol Imaging Cancer* **2021**, *3* (4), No. e200069.

(19) Zalba, S.; Contreras, A. M.; Haeri, A.; Ten Hagen, T. L.; Navarro, I.; Koning, G.; Garrido, M. J. Cetuximab-oxaliplatin-liposomes for epidermal growth factor receptor targeted chemotherapy of colorectal cancer. *J. Controlled Release* **2015**, *210*, 26−38.

(20) Nellis, D. F.; Giardina, S. L.; Janini, G. M.; Shenoy, S. R.; Marks, J. D.; Tsai, R.; Drummond, D. C.; Hong, K.; Park, J. W.; Ouellette, T. F.; et al. Preclinical manufacture of anti-HER2 liposome-inserting, scFv-PEG-lipid conjugate. 2. Conjugate micelle identity, purity, stability, and potency analysis. *Biotechnol. Prog.* **2005**, *21* (1), 221−232.

(21) Fleck, R. A.; Romero-Steiner, S.; Nahm, M. H. Use of HL-60 cell line to measure opsonic capacity of pneumococcal antibodies. *Clin. Diagn. Lab. Immunol.* **2005**, *12* (1), 19−27.

(22) Chen, S. H.; Scott, X. O.; Ferrer Marcelo, Y.; Almeida, V. W.; Blackwelder, P. L.; Yavagal, D. R.; Peterson, E. C.; Starke, R. M.; Dietrich, W. D.; Keane, R. W.; et al. Netosis and Inflammasomes in Large Vessel Occlusion Thrombi. *Front Pharmacol* **2021**, *11*, No. 607287. Pir, G. J.; Parray, A.; Ayadathil, R.; Pananchikkal, S. V.; Mir, F. A.; Muhammad, I.; Abubakar, A.; Amir, N.; Hussain, S.; Haroon, K. H.; et al. Platelet-Neutrophil Association in NETs-Rich Areas in the Retrieved AIS Patient Thrombi. *Int. J. Mol. Sci.* **2022**, *23* (22), 14477.

(23) Collins, S. J.; Ruscetti, F. W.; Gallagher, R. E.; Gallo, R. C. Terminal differentiation of human promyelocytic leukemia cells induced by dimethyl sulfoxide and other polar compounds. *Proc. Natl. Acad. Sci. U. S. A.* **1978**, *75* (5), 2458−2462.

(24) Tan, Q.; Guo, P.; Zhou, J.; Zhang, J.; Zhang, B.; Lan, C.; Xian, J.; Ge, M.; Feng, H.; Chen, Z. Targeting neutrophil extracellular traps enhanced tPA fibrinolysis for experimental intracerebral hemorrhage. *Transl Res.* **2019**, *211*, 139−146.

(25) Kitano, T.; Hori, Y.; Okazaki, S.; Shimada, Y.; Iwamoto, T.; Kanki, H.; Sugiyama, S.; Sasaki, T.; Nakamura, H.; Oyama, N.; et al. An Older Thrombus Delays Reperfusion after Mechanical Thrombectomy for Ischemic Stroke. *Thromb Haemost* **2022**, *122* (3), 415−426.

(26) Crabtree, G. R. Fc receptors of a human promyelocytic leukemic cell line: evidence for two types of receptors defined by binding of the staphylococcal protein A-IgG1 complex. *J. Immunol*

https://doi.org/10.1021/acsomega.4c01525
ACS Omega 2024, 9, 29391−29400

1980, *125* (1), 448−453. Chi, M.; Tridandapani, S.; Zhong, W.; Coggeshall, K. M.; Mortensen, R. F. C-reactive protein induces signaling through Fc gamma RIIa on HL-60 granulocytes. *J. Immunol* **2002**, *168* (3), 1413−1418.

https://doi.org/10.1021/acsomega.4c01525
ACS Omega 2024, 9, 29391−29400